PERGAMON

Computers in Biology and Medicine 29 (1999) 19–38

Computers in Biology and Medicine

A three-dimensional model for arterial tree representation, generated by constrained constructive optimization

Rudolf Karch[a,*], Friederike Neumann[b], Martin Neumann[c], Wolfgang Schreiner[a]

[a]*Department of Medical Computer Sciences, University of Vienna, Spitalgasse 23, A-1090 Wien, Austria*
[b]*Department of Cardiothoracic Surgery, University of Vienna, Währinger Gürtel 18-20, A-1090 Wien, Austria*
[c]*Institute of Experimental Physics, Section for Computational Physics, University of Vienna, Strudlhofgasse 4, A-1090 Wien, Austria*

Received 27 February 1998; accepted 3 November 1998

Abstract

The computational method of constrained constructive optimization (CCO) has been generalized in two important respects: (1) arterial model trees are now grown within a convex, three-dimensional piece of tissue and (2) terminal flow variability has been incorporated into the model to account for the heterogeneity of blood flow observed in real vascular beds. Although no direct information from topographic anatomy enters the model, computer-generated CCO trees closely resemble corrosion casts of real arterial trees, both on a visual basis and with regard to morphometric parameters. Terminal flow variability was found to induce transitions in the connective structure early in the trees' development. The present generalization of CCO offers — for the first time — the possibility to generate *optimized* arterial model trees in three dimensions, representing a realistic geometrical substrate for hemodynamic simulation studies. With the implementation of terminal flow variability the model is ready to simulate processes such as the adaptation of arterial diameters to changes in blood flow rate or the formation of different patterns of angiogenesis induced by changing needs of blood supply.

Keywords: Arterial trees; Anatomic models; Computer simulation; Constrained constructive optimization; Topology

* Corresponding author. Fax: +43-1-40400-6677; e-mail: rudolf.karch@akh-wien.ac.at.

0010-4825/99/$ - see front matter
PII: S0010-4825(98)00045-6

1. Introduction

Arterial vessel trees fulfill the crucial task of efficiently supplying blood to all sites of a given piece of tissue. Based on computer models of arterial trees, hemodynamic simulation studies have been frequently used to gain a better understanding of both diagnostic and therapeutic aspects of blood flow. These simulations employed compartmental representations (e.g. [1, 2]) or branching tube models of arterial trees as their geometrical substrate. Branching tube models are either directly drawn from real anatomical data (e.g. [3–5]) or constructed as self-similar (deterministic or stochastic) networks (e.g. [6–8]). While anatomical models provide an accurate representation of the coarse structure of vascular trees, they clearly cannot cover the morphological details of real vascular trees. On the other hand, self-similar models have been reported to reproduce many statistical properties of real vascular trees. However, these rule-based fractal network models do not accurately represent anatomic features of real vascular networks [8]. Combining the benefits of the conceptually different approaches mentioned above, the method of *constrained constructive optimization* (CCO, [9]) allows to generate in full detail (i.e. providing the coordinates and diameters of vessel segments) highly realistic arterial model trees of some 10^4 vessel segments extending from the feeding artery down to the prearteriolar level. In such a CCO tree, not only the temporal but also the spatial variation of blood flow during the cardiac cycle can be systematically investigated by hemodynamic simulation [10, 11]. The CCO method is based on the principle of optimum design and does not rely on direct anatomical input data from morphometric measurements: the model tree is grown by successively adding new terminal segments while maintaining a set of physiological boundary conditions and constraints; at each step of growth the geometric location and topological site of a new connection is optimized according to a given optimization target function calculated from the whole model tree grown so far.

Previous CCO models were able to reproduce key features of arterial trees, such as segment radii [9] and branching angle statistics [12], as well as pressure profiles [13, 14]. However, the shape of the tissue to be perfused was only modeled in two dimensions (circular and elliptic areas [15, 16]). Therefore, a more realistic modeling calls for a three-dimensional geometric representation of a *volume* instead of a surface to be perfused. This generalization is necessary not only for convex, parynchimatous, solid organs such as the liver or the spleen, but even more for hollow organs like the ventricles of the heart, featuring pronounced differences between outer and inner layers.

Another key restriction of previous CCO models was the assumption that all terminal segments supply their microcirculatory areas at constant flows and pressures. In particular, the equality of terminal flows is unable to reproduce experimental findings on spatial blood flow heterogeneity reported for the myocardium and for single skeletal muscles [17, 18]. In the present algorithm we therefore generalize the concept of CCO to arbitrarily chosen terminal flows. Thus, flow distributions found from measurements in the heart and in skeletal muscles can be prescribed during the model generation and will appear in the fully developed CCO tree. In addition it will be shown that varying terminal flow distributions not only yield different vascular calibers but also induce different geometric structures of the model trees.

2. The method of CCO

2.1. General model characteristics

The generation of arterial model trees within the framework of CCO is essentially based on the following assumptions:

- The portion of tissue to be perfused is modeled as a three-dimensional convex volume (*perfusion volume*).
- The arterial tree is represented as a binary branching network of rigid cylindrical tubes (*segments*), perfused at steady state and laminar flow conditions. Starting at the feeding artery (*root segment*), the tree successively bifurcates down to the prearteriolar level, where the model tree is truncated in the form of *terminal segments*. The latter are considered to feed the microcirculatory network which is not modeled in detail.
- The model tree should fill the space of the perfusion-volume as evenly as possible without intersection of segments.
- Blood is assumed an incompressible, homogeneous Newtonian fluid and the hydrodynamic resistance R_j of each segment j is given by Poiseuille's law (e.g. [19])

$$R_j = \left(\frac{8\eta}{\pi}\right)\frac{l_j}{r_j^4}, \tag{1}$$

where l_j and r_j denote the length and internal radius of segment j and η is the (constant) viscosity of blood. Given R_j, the pressure drop Δp_j along segment j is then determined by the flow Q_j through segment j

$$\Delta p_j = R_j Q_j. \tag{2}$$

The total hydrodynamic resistance R of the model tree is calculated by decomposing the tree into subtrees and recursively employing the respective relations for the resistances of parallel and serial arrangements of tubes.

In addition to the model assumptions given above, basic physiological characteristics of real arterial trees are mapped into a set of *physiological boundary conditions* and *constraints:*

- The pressures p_{term} at the distal ends of terminal segments are equal and assumed to be the inflow pressures into the microcirculatory network.
- Each terminal segment j delivers an individual amount of blood flow $Q_{\text{term},j}$ into the microcirculation against the constant terminal pressure p_{term}.
- The laminar flow resistance of the whole tree induces a given total perfusion flow Q_{perf} across the overall pressure drop

$$\Delta p = p_{\text{perf}} - p_{\text{term}}, \tag{3}$$

where p_{perf} denotes the perfusion pressure in the feeding artery. The net flow Q_{perf} is the same for each step of tree generation.

- N_{term} terminal segments, yielding

$$N_{\text{tot}} = 2N_{\text{term}} - 1 \tag{4}$$

segments in total, are arranged in such a way that their distal ends are evenly distributed within the perfusion volume.
- At bifurcations the radii of parent and left and right daughter segments obey a power law (*bifurcation law*) of the form (e.g. [20])

$$r_{\text{parent}}^{\gamma} = r_{\text{left}}^{\gamma} + r_{\text{right}}^{\gamma} \tag{5}$$

with a constant exponent $\gamma > 0$ (*bifurcation exponent*). This relation determines the shrinkage of segment radii across bifurcations (or the amount of expansion in the cross sectional areas of parent and daughter segments).

As could be shown for the CCO method [22], all physiological boundary conditions and constraints regarding pressures, flows and the bifurcation law, Eq. (5), can simultaneously be fulfilled by appropriate scaling of segment radii, regardless of the particular geometrical and topological structure of a given model tree.

2.2. Algorithm of tree generation

The algorithm of tree generation starts with a randomly placed perfusion site for the distal end of the first segment (which is at the same time root and terminal segment). Its proximal end represents the fixed inlet for the feeding artery at the surface of the perfusion volume. Further growth of the model tree is accomplished by successively adding new terminal segments, each of which connects a randomly chosen point within the perfusion volume to one of the existing segments, thus forming a new bifurcation somewhere along that segment. Since the two-dimensional CCO method has been described in detail in previous papers [9, 22], only the major points of the algorithm will be restated here for ease of reference.

First, a Cartesian coordinate point $\mathbf{x}_{inew}$ is drawn from a pseudo-random number sequence with a spatially uniform probability distribution. $\mathbf{x}_{inew}$ is accepted as a candidate for a new terminal location only if both $\mathbf{x}_{inew}$ is in the interior of the perfusion volume and the distance of $\mathbf{x}_{inew}$ to all segments generated so far exceeds an adaptive threshold value $d_{\min}$ (*distance criterion*), i.e. $d_{\min}$ is properly decreased when the total number of segments — and hence the 'resolution' of the tree — increases during the course of tree generation. Once $\mathbf{x}_{inew}$ has been accepted as a new terminal site, it is tentatively connected to the midpoints of a fixed number (N_{con}) of segments in the spatial vicinity of $\mathbf{x}_{inew}$ (*connection search*). However, adding a new terminal segment *inew*, i.e. generating a new bifurcating segment *ibif*, disturbs the distribution of segmental flows, thus violating the boundary condition regarding the terminal flows $Q_{\text{term},j}$. In order to reestablish the correct terminal flows, the hydrodynamic resistance of the tree must be adjusted. As the lengths of the segments as well as the terminal and perfusion pressures are fixed, this can only be accomplished by proper rescaling of the segments' radii for each temporary connection (cf. Fig. 1, upper panel).

Since the terminal pressures are assumed equal, the flow splitting ratio at the bifurcating segment *ibif* is given by (cf. Eq. (2))

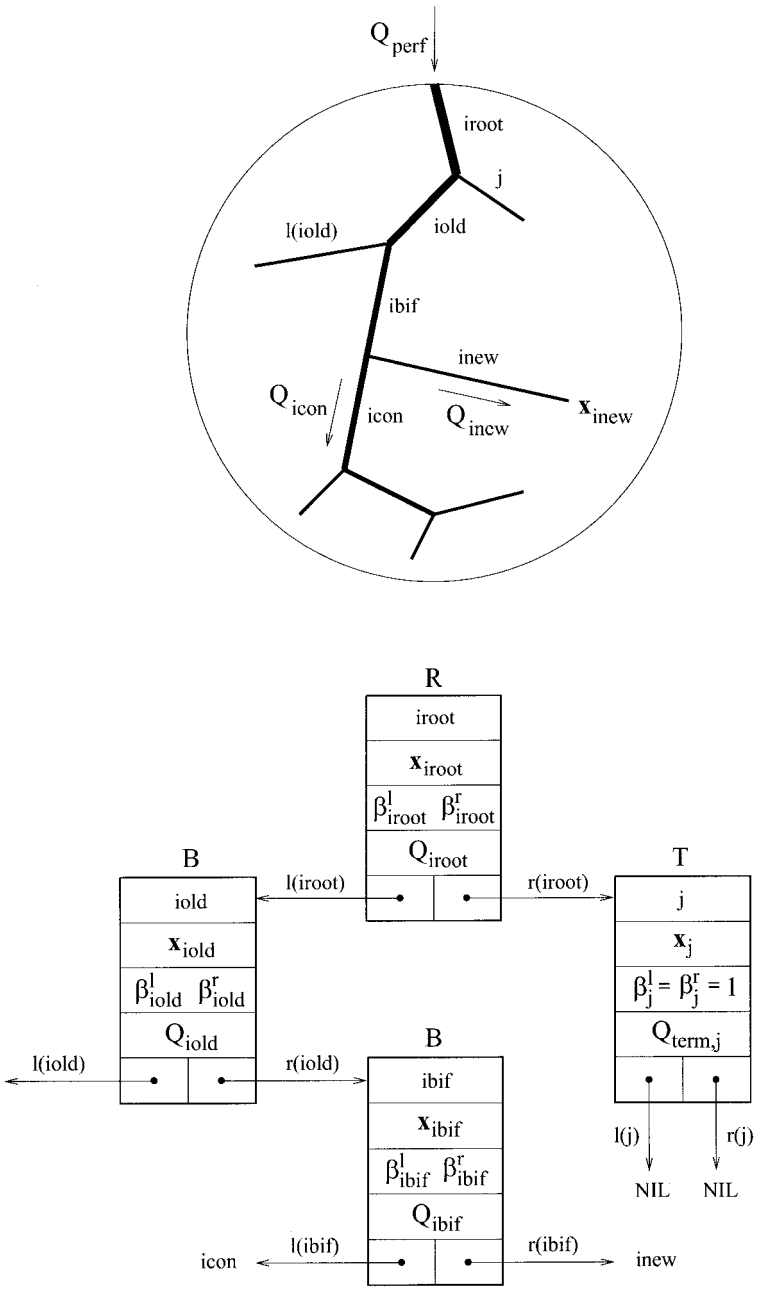

Fig. 1. Schematic display of the CCO binary tree model. Upper panel: adding a new terminal segment *inew* to a selected preexisting segment *icon* generates a new bifurcating segment *ibif*. Lower panel: corresponding data structure for the internal representation of CCO trees. In addition to its index i and left and right pointers (l(i), r(i)), each node i holds the segment's coordinates $\mathbf{x}_i$, left and right bifurcation ratios $\beta_i{}^{\mathrm{l}}$ and $\beta_i{}^{\mathrm{r}}$, as well as the flow Q_i through segment i. The three segment-types are indicated by R for the root segment, B for bifurcating segments and T for terminal segments.

$$\frac{Q_{icon}}{Q_{inew}} = \frac{R_{inew}}{R_{\mathrm{sub},icon}} = \frac{R^*_{inew}/r^4_{inew}}{R^*_{\mathrm{sub},icon}/r^4_{icon}}, \tag{6}$$

where $R_{\mathrm{sub},icon}$ is the hydrodynamic resistance of segment *icon* including its left and right subtrees and R_{inew} is the resistance of the new terminal segment *inew*; $R^*_{\mathrm{sub},icon} = R_{\mathrm{sub},icon} r^4_{icon}$ and $R^*_{inew} = R_{inew} r^4_{inew}$ are the corresponding reduced hydrodynamic resistances. This factorization is convenient, because we assume that $R^*_{\mathrm{sub},icon}$ is independent of r_{icon}, i.e. the bifurcation ratios β_j (see below) in the subtree distal to *icon* remain constant and unaffected by the addition of *inew*. Whereas R^*_{inew} is simply $8\eta l_{inew}/\pi$, the reduced hydrodynamic resistance $R^*_{\mathrm{sub},icon}$ of segment *icon* is calculated by recursively traversing the subtrees of *icon* in postorder mode (i.e. first traversing the left subtree, then the right subtree and finally visiting *icon* [36]) and applying the following relation at each node *j*:

$$R^*_{\mathrm{sub},j} = \left(\frac{8\eta}{\pi}\right) l_j + \left[\frac{(r_{\mathrm{left},j}/r_j)^4}{R^*_{\mathrm{left},j}} + \frac{(r_{\mathrm{right},j}/r_j)^4}{R^*_{\mathrm{right},j}}\right]^{-1}. \tag{7}$$

$R^*_{\mathrm{left},j}$ is the reduced resistance and $r_{\mathrm{left},j}$ is the inlet radius of the left subtree of segment *j*. Eq. (6) yields the ratio for the radii of the daughter segments of the bifurcating segment *ibif*

$$\frac{r_{icon}}{r_{inew}} = \left(\frac{Q_{icon} R^*_{\mathrm{sub},icon}}{Q_{inew} R^*_{inew}}\right)^{1/4}. \tag{8}$$

Using the bifurcation rule (Eq. (5)), one obtains the 'bifurcation ratios' with respect to segment *ibif*

$$\beta^{icon}_{ibif} = \frac{r_{icon}}{r_{ibif}} = \left[1 + \left(\frac{r_{icon}}{r_{inew}}\right)^{-\gamma}\right]^{-1/\gamma} \tag{9}$$

and

$$\beta^{inew}_{ibif} = \frac{r_{inew}}{r_{ibif}} = \left[1 + \left(\frac{r_{icon}}{r_{inew}}\right)^{\gamma}\right]^{-1/\gamma}. \tag{10}$$

The last equations guarantee that the flows split correctly between the subtree distal to *ibif* and the new terminal segment *inew*. In the case of equal terminal flows, the flow splitting ratio Q_{icon}/Q_{inew} is obtained by counting the number of terminal segments in the subtrees distal to *icon*; for variable terminal flows, weighted sums are used instead. Thus, the bifurcation ratios β_{ibif} are uniquely determined by the terminal flows and by the geometry of the tree generated so far. However, the new bifurcating segment *ibif* now has to accommodate the additional flow through the new terminal segment *inew*. Hence, the respective bifurcation ratios r_{ibif}/r_{iold} and $r_{\mathrm{l}(iold)}/r_{iold}$ must be recalculated by means of the equations given above. The same argument holds for all bifurcations proximal to *ibif*, so the tree has to be traversed up to the root segment, starting at *ibif*, to recalculate the corresponding bifurcation ratios. Since only the *ratios* of the respective radii are considered, there is no need to store their *absolute* values every time a bifurcation ratio is adjusted. Should the absolute value r_j for the radius of segment *j* be required, it can easily be

obtained from

$$r_j = r_{iroot} \prod_{k=j}^{iroot} \beta_k, \tag{11}$$

where β_k are the corresponding bifurcation ratios and the product is extended over all bifurcating segments on the unique path from segment j to the root segment *iroot*. The radius of the root segment r_{iroot} is given by

$$r_{iroot} = \left(\frac{R^*_{\mathrm{sub},iroot}}{R_{\mathrm{sub},iroot}} \right)^{1/4} = \left[R^*_{\mathrm{sub},iroot} \frac{Q_{\mathrm{perf}}}{(p_{\mathrm{perf}} - p_{\mathrm{term}})} \right]^{1/4}, \tag{12}$$

where $R_{\mathrm{sub},iroot} = R$ denotes the hydrodynamic resistance of the whole tree.

Each new bifurcation at the temporary connection sites $j = 1, \ldots, N_{\mathrm{con}}$ is geometrically optimized (see Section 2.3). The results for each of these temporary connections regarding optimization (the value of the target function in its minimum) and geometry (e.g. segment intersections) are recorded in line j of a neighborhood table established for $\mathbf{x}_{inew}$ (*connection evaluation table*, CET) and the new bifurcation is removed. After having tested all possible connections in the neighborhood of $\mathbf{x}_{inew}$, the CET is scanned and reduced to the subset $\mathrm{CET_r}$ of all reasonable connections. Unless $\mathrm{CET_r}$ is the empty set (in which case the tossing for a new terminal location is repeated), the optimum (in terms of a cost function) connection in $\mathrm{CET_r}$ is adopted as permanent for the new terminal site $\mathbf{x}_{inew}$. The above procedure of successively adding new terminal segments is repeated until the preset maximum number of terminals N_{term} is achieved, which in turn defines the 'resolution' of the model tree. Fig. 2 gives a flow chart of the CCO algorithm.

2.3. Geometric and structural optimization

Arterial trees serve the purpose of efficiently carrying blood to all sites of tissue, representing a fluid transport system costly to construct and to maintain [23]. Assuming that growth and structure of arterial trees are not purely arbitrary but governed by optimality principles [24–28], the question arises which principles to adopt for a computer model to be physiologically reasonable. Several approaches related to functional optimality of arterial trees have been reported in the literature (e.g. [24, 29–34]). To numerically characterize the degree of optimality of a given tree, a cost (or target) function must be selected. In the present study we consider the following generalized form for the target function T_j of a single vessel segment j:

$$T_j = l_j^{\mu} r_j^{\lambda}, \tag{13}$$

where λ and μ are constants reflecting the dimensionality of T_j (e.g. setting $\lambda = 2$ and $\mu = 1$ renders T_j proportional to the volume of segment j). If we further assume that the target functions for all vessel segments are *additive*, the total target function T of a whole tree can be written as

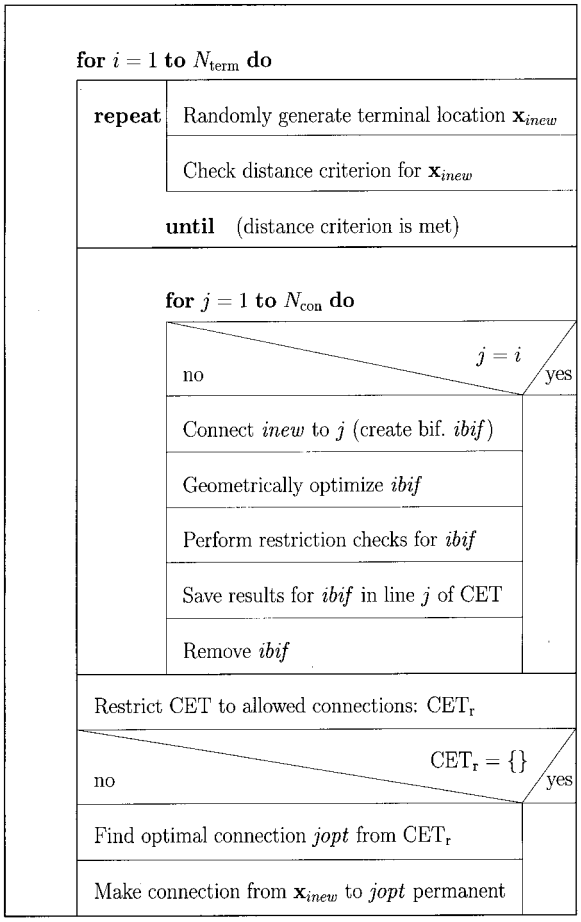

Fig. 2. Algorithm of tree generation. After successfully tossing for a new terminal location $\mathbf{x}_{inew}$, a predefined number N_{con} of existing segments is probed for a potential new permanent bifurcation by tentatively connecting $\mathbf{x}_{inew}$ to each of these segments and geometrically optimizing the locations of the resulting bifurcations. The connection with the smallest value of the target function is adopted as a new permanent bifurcation.

$$T = \sum_{j=1}^{N_{\text{tot}}} T_j. \tag{14}$$

Note that additivity restricts T to a certain family of target functions, while any nonadditive quantities, such as the total hydrodynamic resistance (cf. Eq. (7)), are ruled out as candidates for T.

The method of CCO involves both local (geometric) and global (structural) aspects of optimization: when a new terminal site is temporarily connected to an existing segment, the location of the resulting bifurcation is optimized with respect to the target function T (*geometric optimization*). Once the connection corresponding to the smallest value of T has been identified in the respective CET during the connection search process, this connection is made permanent, which in turn defines the 'global' minimum of T and the connective structure

of the tree (*structural optimization*). Thus, minimizing T not only determines the geometric location of single bifurcations, but also controls the global topological structure of the model trees and both aspects are governed by the very same target function T.

Geometrically optimizing the location of a single bifurcation requires to find the local minimum of T subject to a set of *geometrical restrictions*:

- The bifurcation must stay in the interior of the perfusion volume.
- The lengths of the three segments forming the bifurcation must not degenerate.

These geometrical restrictions have to be fulfilled in addition to the physiological boundary conditions and constraints (cf. Section 2.1). Since the process of finding the local minimum of T involves moving the position of the bifurcation being optimized, the lengths (and consequently the hydrodynamic resistances) of the three segments directly attached to it will change. This again violates the boundary conditions regarding the distribution of flows. Therefore, all bifurcation ratios affected (i.e. the ratios for the daughter segments of the bifurcation being moved, cf. Eqs. (9) and (10), as well as the respective ratios for all bifurcations along the path to the root segment) and the radius of the root segment have to be simultaneously rescaled while a single bifurcation is geometrically optimized. Hence, the change in T during the displacement of a single bifurcation is caused both by altering the segments' lengths of that bifurcation and by rescaling the radii of a whole subset of segments in the rest of the tree.

Virtual movements of a single bifurcation — while still maintaining the physiological constraints — change the value of the target function for the model tree, thus generating a *three-dimensional* scalar field. However, the final (i.e. optimum) positions of the bifurcations in our model trees were always found to lie in the plane defined by the endpoints of the respective three neighboring segments (*bifurcation plane*). This finding is consistent with results reported for the arterial network of the human heart [35]. Restricting the virtual movements of the bifurcation to its corresponding bifurcation plane, the target function of the model tree can be represented as a two-dimensional surface plot (cf. Fig. 3). Note that one obtains a separate plot for each bifurcation, and for a given bifurcation the respective surface plots will differ as the tree is grown to its final size.

3. Implementation

The model tree is most naturally represented in the memory of the computer as a linked binary tree (e.g. [36]). First, each segment is assigned an arbitrary but unique index j. The connective structure of the tree is defined by means of node pointers l(j) and r(j), which hold the indices of the 'left' and 'right' daughters of segment j. The geometry of the tree is characterized by the Cartesian coordinates $\mathbf{x}_j$ of the distal endpoint of each segment j together with its actual (inner) radius r_j. Rather than storing the segments' radii, the respective left and right bifurcation ratios β_j^{l} and β_j^{r} are kept in memory (for terminal segments, these ratios are set to unity). Fig. 1 (lower panel) illustrates the resulting data structure for the model trees.

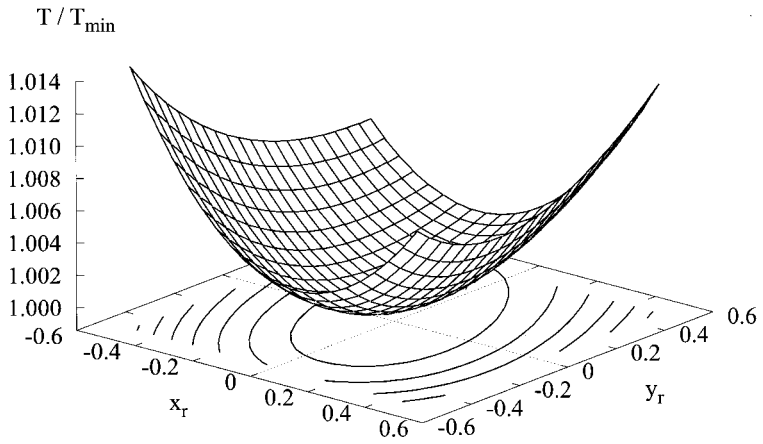

Fig. 3. Surface plot representing the changes in the target function T of the whole tree when moving a selected bifurcation during its geometric optimization. The virtual moves of the bifurcation are restricted to its corresponding bifurcation plane. The bifurcation coordinates in this plane, x_r and y_r, are displayed relative to their values at the local minimum T_{min} of T and the target function is normalized with respect to T_{min}.

Since the locations of new terminal segments being added to a preexisting tree should be selected on a stochastic basis, a pseudo-random number generator (NAG-routine G05CAF [37]) with a uniform probability distribution between 0 and 1 was used to obtain — after appropriate scaling — the respective segment coordinates.

The terminal flows $Q_{term,j}$ can either be set to a constant fraction of the total perfusion flow, $Q_{term,j} = Q_{perf}/N_{term}$, or their values can be selected at random with a prescribed probability distribution, normalized so as to yield $\sum_{j=1}^{N_{term}} Q_{term,j} = Q_{perf}$.

The geometrical optimization of a single bifurcation under the physiological constraints and geometrical restrictions previously mentioned was implemented by means of a constrained nonlinear optimization algorithm, as supplied with the NAG-library routine E04UCF [37]. For a bifurcation consisting of the three segments *ibif*, *icon* and *inew* (cf. Fig. 1, upper panel), the nonlinear constraints in E04UCF together with their lower and upper bounds were chosen as follows:

$$\begin{pmatrix} 0 \\ 2r_{ibif} \\ 2r_{icon} \\ 2r_{inew} \end{pmatrix} \leq \begin{pmatrix} \|\mathbf{x}_{ibif}\| \\ \|\mathbf{x}_{ibif} - \mathbf{x}_{iold}\| \\ \|\mathbf{x}_{icon} - \mathbf{x}_{ibif}\| \\ \|\mathbf{x}_{inew} - \mathbf{x}_{ibif}\| \end{pmatrix} \leq \begin{pmatrix} r_{perf} \\ +\infty \\ +\infty \\ +\infty \end{pmatrix}, \tag{15}$$

where a spherical perfusion volume (radius r_{perf}) centered at the origin has been assumed. The first line in Eq. (15) reflects the constraint regarding the position of the bifurcation within the perfusion volume, whereas the remaining lines require that the lengths of the three segments forming the bifurcation must not degenerate to zero; this was achieved by setting the lower bounds for the lengths to twice the corresponding segment radii prior to optimization.

A three-dimensional intersection check of arterial segments was implemented by considering the mutual penetration of respective cylinder-sections. Checking for segment intersections is performed only after the optimization step; this procedure allows for segments being still

eligible to form a new bifurcation, even though they might have penetrated into others during the optimization moves.

During the connection search for a new terminal location $\mathbf{x}_{inew}$ a neighborhood table (CET) assigned to $\mathbf{x}_{inew}$ is employed to assess each tentative connection. In the current implementation of CCO the initial size N_{con}^{0} of the CET was set to a fixed value. If no candidate for a permanent connection is found within the actual CET, its size is gradually enlarged. Only if the constant upper limit $N_{\mathrm{con}}^{\max}$ for the size of the CET is reached without identifying a permanent connection, the current terminal location is dropped and the tossing for $\mathbf{x}_{inew}$ is repeated. Fig. 4 illustrates the frequency distribution of the CET-index for permanent connections sampled during the growth of a complete model tree without setting an upper limit for the size of the neighborhood table. As Fig. 4 suggests, $N_{\mathrm{con}}^{0} = 20$ represents a reasonable choice for the initial size of the CET. Since the indices in the CET of the segments to probe for a permanent connection are arranged in ascending order with respect to the distance between $\mathbf{x}_{inew}$ and the midpoint of the segment in question, Fig. 4 indicates that the segment closest to $\mathbf{x}_{inew}$ is also the most probable candidate for a permanent connection with $\mathbf{x}_{inew}$. Finally, the constant size of the CET has an important impact on the overall computational performance of the algorithm: since the processor time spent to probe all segments in a CET is practically independent of the actual size of the tree, CCO essentially represents an $O(n)$ algorithm, adequate for being used in larger problems.

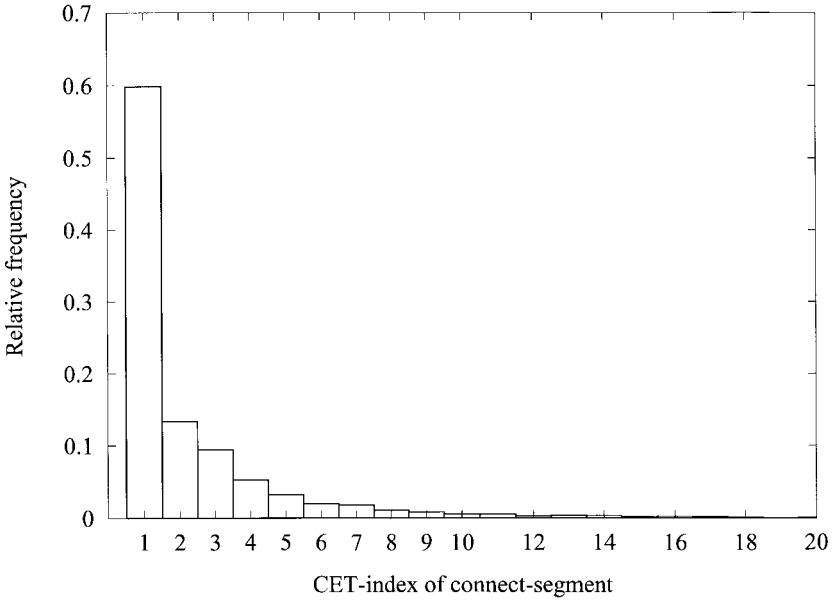

Fig. 4. Relative frequency of CET-index for permanent connections. Every new terminal location $\mathbf{x}_{inew}$ is assigned a neighborhood table (connection evaluation table, CET), and the indices of the segments in these tables are sorted in ascending order with regard to the spatial distance of $\mathbf{x}_{inew}$ to the midpoint of the respective segment. The resulting frequency distribution suggests that the most probable candidates for permanent connections are the segments in the close vicinity of $\mathbf{x}_{inew}$.

4. Results and discussion

4.1. 3-D representation of tree development

The new three-dimensional CCO method was used to simulate the arterial tree of a spherical model tissue under the following physiological conditions: perfusion pressure $p_{perf} = 100$ mm Hg, terminal pressure $p_{term} = 60$ mm Hg and total perfusion flow $Q_{perf} = 500$ ml/min (cf. Table 1). This choice of model parameters represents an arterial tree supplying approximately 100 g of myocardial tissue under maximum vasodilation (cf. [22]). The number of terminal segments $N_{term} = 4000$ was chosen in order to allow for a very realistic appearance of the model trees, yet feasible even on medium-size computer facilities.

The bifurcation exponent (cf. Eq. (5)) was set to $\gamma = 3$. This value for γ is suggested by theoretical arguments (e.g. [20, 21]) and was approximately confirmed from measurements on real arterial trees [35, 38].

Since the total intravascular volume V of the tree is a generally accepted choice for an optimization target function (e.g. [27]), the free parameters λ and μ in Eq. (13) were set accordingly ($\lambda = 2$ and $\mu = 1$), thus leaving T proportional to V.

Fig. 5 illustrates the development of a three-dimensional CCO model tree optimized for minimum intravascular volume at equal terminal flows $Q_{term} = Q_{perf}/N_{term}$. Panels a–d correspond to $N_{term} = 20$, 200, 1000 and 4000 terminal segments; for the simulation parameters see Table 1. From visual inspection of Fig. 5 it is immediately evident that the locations of the very first terminal segments determine the coarse structure of the fully developed model tree. This is due to the fact that segments originating from early stages of development become mainstream vessels when the tree is grown to its final size.

Table 1
Global model parameters

Parameter	Meaning	Value
V_{perf}	perfusion volume	100 cm^3
p_{perf}	perfusion pressure	100 mm Hg
p_{term}	terminal pressure	60 mm Hg
Q_{perf}	perfusion flow	500 ml/min
N_{term}	number of terminals	4000
Q_{term}	terminal flow	0.125 ml/min[a]
η	viscosity of blood	3.6 cp
γ	bifurcation exponent	3
λ	exponent of r_j in T_j	2
μ	exponent of l_j in T_j	1
N_{con}^{0}	initial size of CET	20
N_{con}^{max}	maximum size of CET	40

[a] For equal terminal flows and $N_{term} = 4000$.

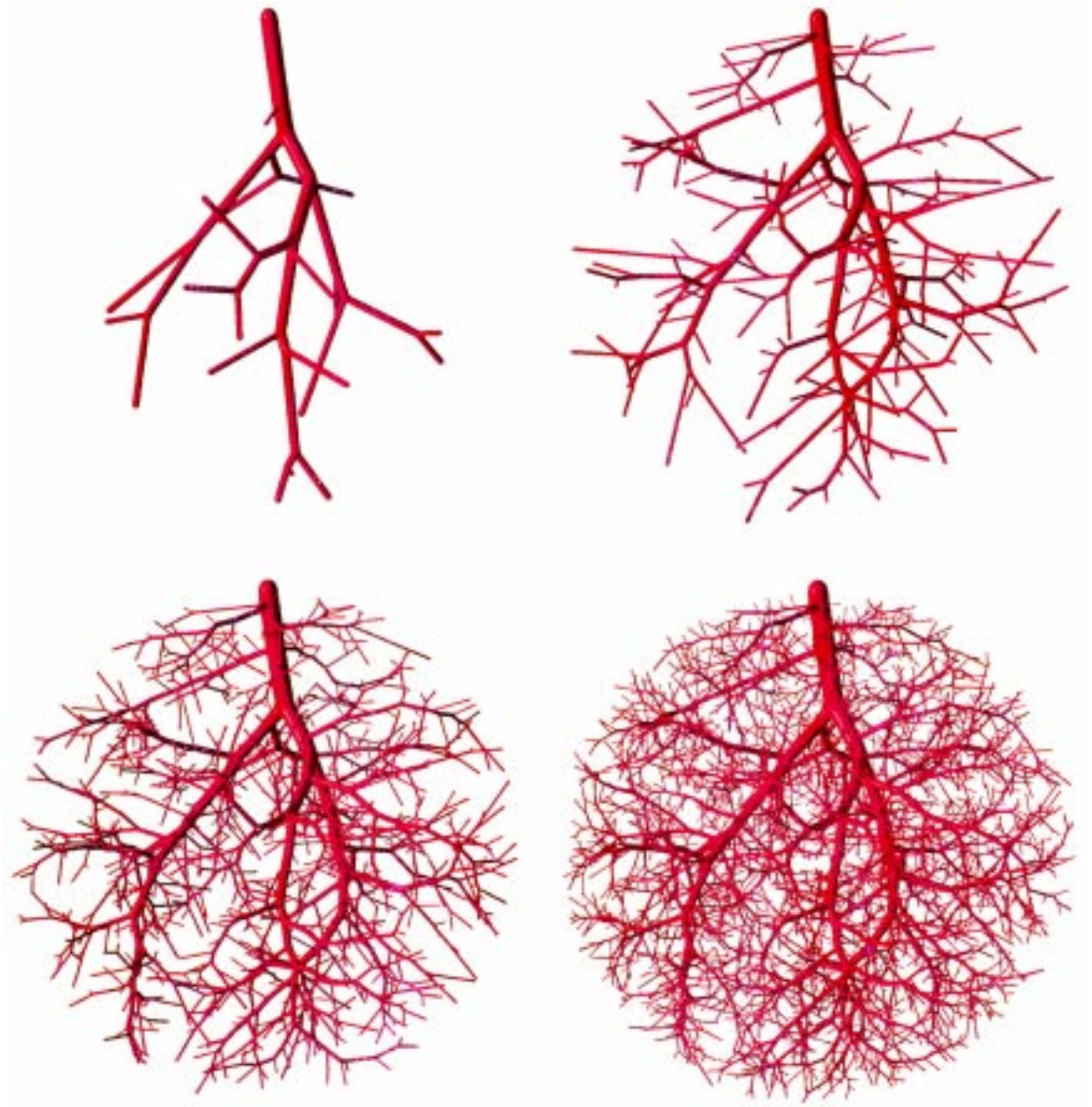

Fig. 5. Visual representation of tree development. The 4 panels show stages of development (20, 200, 1000, 4000 terminal segments, respectively) of a CCO model tree optimized for minimum intravascular volume at $Q_{\text{term}} = \text{const.}$ and simulation parameters of Table 1. Segments originating from the first stages of development (upper left) eventually become the mainstream vessels in the final tree (lower right). Visualization was performed by representing the vessel segments as the iso-surface of a pseudopotential assigned to the whole tree (cf. [40]) and using image-based direct volume rendering. Computing time for $N_{\text{term}} = 4000$ was approx. 10 h on a DEC-Alpha 21164/333 MHz CPU.

4.2. Comparison with experimental data

In order to compare the computer-generated model trees with real arterial trees on a morphometric basis, we used data reported by Zamir and Chee [39]. Fig. 6 shows the mean diameter and standard deviation (S.D.) of all vessel segments at a certain 'bifurcation level' (defined as the number of proximal bifurcations along the path from the respective segment to the root segment), calculated for a CCO model tree with $N_{\text{term}} = 250$ terminal segments (i.e. 499 segments in total) and with p_{term} set to 72 mm Hg to yield the same radius of the root segment as for $N_{\text{term}} = 4000$; the remaining simulation parameters were those given in Table 1. The choice of N_{term} approximately reflects the number of segments measured in the experimental study of Zamir and Chee [39]. Fig. 6 indicates that both the mean segment diameter and the range of diameters (i.e. their S.D.) within each level decrease very similar to the experimental results. The model predictions for the diameter of the root segment (at level 0), as well as the mean diameters for bifurcation levels 1–3 and higher than 7 are in good agreement with the experimental data, while the model slightly underestimates the mean vessel diameters of bifurcation levels in between (levels 4–7).

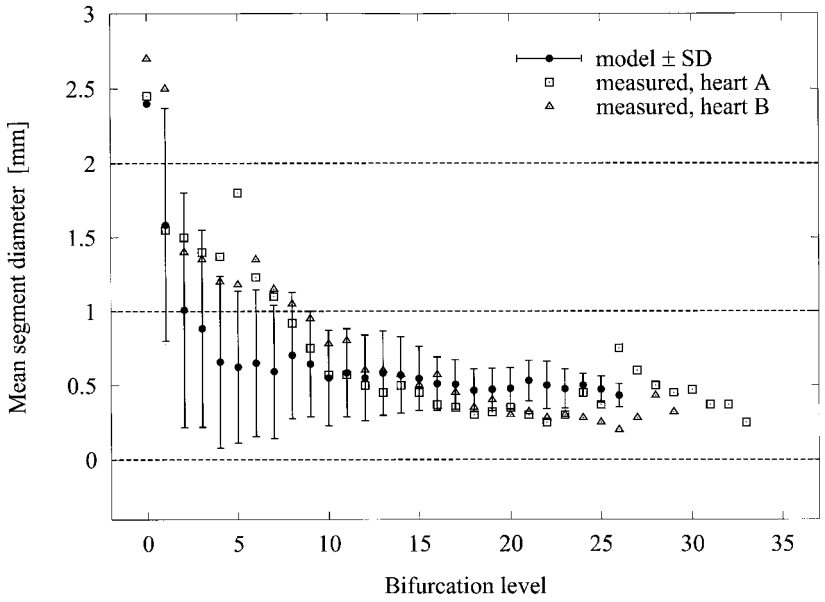

Fig. 6. Averaged segment diameters at respective bifurcation levels. Solid circles indicate the mean diameters of all vessel segments at a certain bifurcation level (defined as the number of proximal bifurcations). These data points were calculated from a CCO model tree with 250 terminal segments (499 segments in total) and with p_{term} set to 72 mm Hg. The remaining simulation parameters were identical to those used for Fig. 5 (cf. Table 1). Vertical bars represent standard deviations (S.D.) from the mean diameter values. Open squares and triangles denote measurements from corrosion casts of the coronary networks of two human hearts [39].

4.3. Flow distribution influences model structure

Experimental results indicate that blood flow in the myocardium and in skeletal muscles exhibits considerable heterogeneity [17, 18]. Therefore, one major generalization achieved in the present work is the possibility to allow for an arbitrary, predefined distribution of terminal flows as a physiologically more realistic boundary condition, compared with previous CCO.

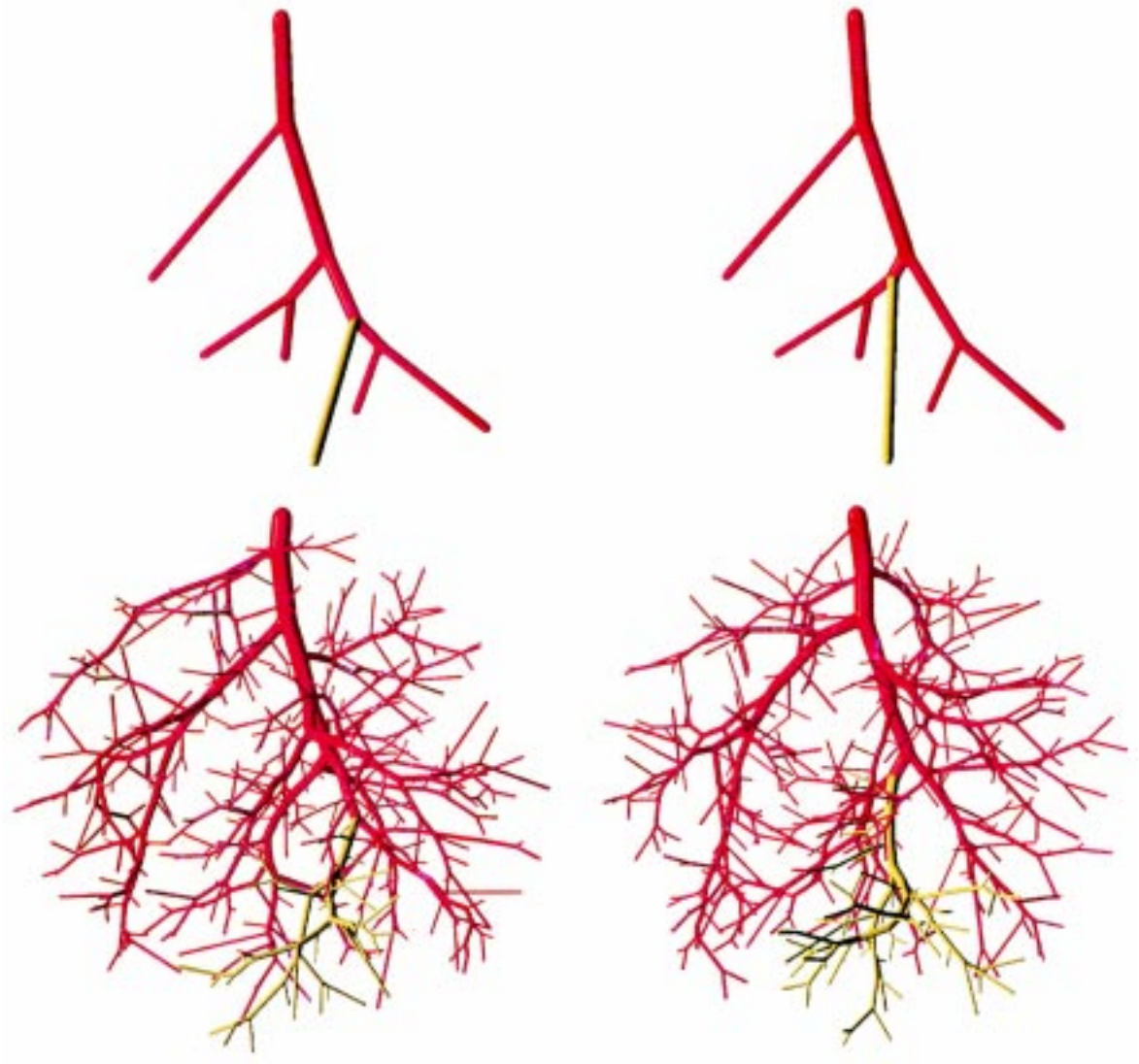

Effects of terminal flow variability on topological structure. Left panels: 'conventional' CCO. Right panels: uniform probability distribution for terminal flows (mean = Q_{perf}/N_{term}, relative dispersion = 20%). Simulation parameters for the generated trees were identical (cf. Table 1), except for the terminal flows. After adding the sixth terminal segment, topologies begin to diverge (upper panels) and lead to substantially different structures when the trees are grown to $N_{term} = 400$ terminal segments (lower panels). The subtrees which emerge from the segments that caused the first transition in topological structures are represented in a different color.

The left panels in Fig. 7 were generated with equal terminal flows ('conventional' CCO), whereas the right panels were obtained by choosing a uniform probability distribution for the terminal flows with a mean value of $\mu_Q = Q_{\mathrm{perf}}/N_{\mathrm{term}}$. Terminal flows were sampled from the interval $(\mu_Q \pm \sqrt{3}\sigma_Q)$ with $\sigma_Q = \mu_Q/5$, i.e. with a relative dispersion of 20% ($=100 \times$ standard deviation σ_Q divided by the mean μ_Q); all other simulation parameters were identical (Table 1). In both cases, the same sequence of pseudo-random numbers was used for generating new terminal locations.

It was interesting to notice that a different distribution of terminal flows gives rise to a transition in the connective structure of the trees at an early stage of development (when the trees were grown to only 11 segments in total, see Fig. 7, top). This switch in structure is due to the fact that (even for identical locations of terminal sites) different flows result in different vascular calibers (cf. Eqs. (8)–(10)) and therefore in slightly different geometries. Because of such small 'perturbations' in the vicinity of a new terminal location, the optimum connection site is now found at a different segment. (A similar behavior is frequently encountered in the field of stochastic simulations, e.g. when the evolution of the system starts to diverge after only a single logical decision due to a slightly different environment).

Once the first topological difference between the two trees has occurred, their connective structures gradually diverge and follow completely different evolutionary paths (Fig. 7, bottom). To emphasize the variations in topology and to clearly trace the different evolutionary paths, we separately consider all descendants of that segment j_1, which induced the first structural transition. In fact, these descendants form the subtree distal to segment j_1, shown in a different color in the fully developed trees ($N_{\mathrm{term}} = 400$).

In summary, it was possible to demonstrate that CCO with variable terminal flow distributions can model several key features of real vascular systems. First, changes in flow distribution in the model primarily affect vessel radii, in analogy to the adaptation of vascular calibers to changing flow distributions in real vascular systems [41–43] (a well-known example being patients with arteriovenous shunts [44]). Second, different paths of model-development correspond to changing patterns of angiogenesis in vivo, as induced by changing needs for blood supply (flow) [45, 46]. Finally, the present extension of the CCO algorithm (variable terminal flows) allows to simulate the vascular reactions due to therapeutic interventions such as shunting and revascularization, both of which drastically redistribute blood flow.

5. Summary

The computational method of constrained constructive optimization has been generalized in two crucial aspects: (1) to grow arterial model trees within a convex, three-dimensional piece of tissue and (2) to incorporate flow heterogeneity known from real vascular beds. The method of CCO — both in the original and the present extended algorithm — basically consists of two tightly coupled steps: (1) growth ('construction') and (2) constrained optimization: the arterial network is modeled as a binary branching tree of nonintersecting, rigid cylindrical tubes, perfused at steady-state and laminar flow conditions and subjected to a set of physiologic boundary conditions and constraints, which are required to be fulfilled at every stage of tree generation. The model tree is grown by repeatedly adding new terminal segments from evenly

distributed and randomly chosen terminal perfusion sites while optimizing the geometric location and topological site of each new bifurcation according to minimum total intravascular volume.

For the generalization to three dimensions, several new concepts have been added to the CCO algorithm: (1) a neighborhood table with an adaptive size, which proved indispensable in the light of computational performance, since efficiency in three-dimensional CCO is even more important than for the two-dimensional case; (2) the possibility to retrace the results of every tentative connection regarding optimality and geometry during the process of finding a new permanent connection and (3) a three-dimensional intersection check for arterial segments of finite thickness. In addition to using a neighborhood table, an efficient and robust algorithm for constrained nonlinear optimization was necessary to guarantee a feasible runtime of three-dimensional CCO.

Although no direct information from topographic anatomy is built into the model, the generated three-dimensional trees closely resemble — on the basis of visual inspection — corrosion casts of real arterial trees. A first comparison regarding the distribution of mean segment diameters over bifurcation levels shows good agreement with experimental data. Moreover, the positions of geometrically optimized bifurcations were always found to lie in the respective bifurcation plane, consistent with experimental results.

The extension of CCO to allow for an arbitrary, predefined distribution of terminal flows adds another realistic feature to the model. In a qualitative assessment, terminal flow variability was found to induce a transition in the connective structure early in the trees' development.

The generalization of CCO to three dimensions offers — for the first time — the possibility to generate *optimized* arterial model trees for three-dimensional organs with an arbitrary convex shape, representing a realistic geometrical substrate for hemodynamic simulation studies. Promising applications which draw on the novel concept of flow variability within the framework of CCO are expected in the following fields: (1) adaptation of arterial diameters to changes in blood flow rate, (2) formation of different patterns of angiogenesis induced by changing needs of blood supply and (3) vascular reactions due to therapeutic interventions such as shunting and revascularization. Other interesting applications of CCO models include the arterial networks of the liver (as a three-dimensional convex perfusion domain) and the retina (as a two-dimensional curved area).

Work is in progress for various enhancements of the present algorithm, in particular regarding nonconvex perfusion domains, improved boundary conditions, and the ability to model intra-organ variations in vascular structure, such as the differences encountered between epi- and endocardial layers of the heart.

References

[1] Y. Sun, H. Gewirtz, Estimation of intramyocardial pressure and coronary blood flow distribution, Am. J. Physiol. 255 (1988) H664–H672 (Heart Circ. Physiol. 24).

[2] P. Bruinsma, T. Arts, J. Dankelman, J.A.E. Spaan, Model of the coronary circulation based on pressure dependence of coronary resistance and compliance, Basic Res. Cardiol. 83 (1988) 510–524.

[3] E. VanBavel, J.A.E. Spaan, Branching patterns in the porcine coronary arterial tree: estimation of flow heterogeneity, Circ. Res. 71 (1992) 1200–1212.
[4] T. Onuki, S. Nitta, Computer simulation of geometry and hemodynamics of canine pulmonary arteries, Ann. Biomed. Eng. 21 (1993) 107–115.
[5] G.S. Kassab, J. Berkley, Y.C. Fung, Analysis of pig's coronary arterial blood flow with detailed anatomical data, Ann. Biomed. Eng. 25 (1997) 204–217.
[6] B. Dawant, M. Levin, A.S. Popel, Effect of dispersion of vessel diameters and lengths in stochastic networks. I. Modeling of microcirculatory flow, Microvasc. Res. 31 (1986) 203–222.
[7] G. Pelosi, G. Saviozzi, M.G. Trivella, A. L'Abbate, Small artery occlusion: a theoretical approach to the definition of coronary architecture and resistance by a branching tree model, Microvasc. Res. 34 (1987) 318–335.
[8] J.H.G.M. Van Beek, S.A. Roger, J.B. Bassingthwaighte, Regional myocardial flow heterogeneity explained with fractal networks, Am. J. Physiol. 257 (1989) H1670–H1680 (Heart Circ. Physiol. 26).
[9] W. Schreiner, Computer generation of complex arterial tree models, J. Biomed. Eng. 15 (1993) 148–149.
[10] M. Neumann, F. Neumann, R. Karch, W. Schreiner, Spatially resolved simulation of coronary hemodynamics, in: M. Cerrolaza, D. Jugo, C.A. Brebbia (Eds.), BIOSIM 96 Proceedings of the 1st Int. Conf. on Simulation Modelling in Bioengineering, Mérida, Venezuela, 1996, Computational Mechanics Publications, Southampton, 1996, pp. 39–51.
[11] M. Neumann, F. Neumann, R. Karch, W. Schreiner, Size and discretization effects in simulations of coronary hemodynamics, in: H. Power, C.A. Brebbia, J. Kenny (Eds.), BIOMED 97 Proceedings of the Fourth Int. Conf. on Computer Simulations in Biomedicine, Acquasparta, Italy, 1997, Computational Mechanics Publications, Southampton, 1997, pp. 23–35.
[12] W. Schreiner, M. Neumann, F. Neumann, S.M. Roedler, A. End, P. Buxbaum, M.R. Müller, P. Spieckermann, The branching angles in computer-generated optimized models of arterial trees, J. Gen. Physiol. 103 (1994) 975–989.
[13] W. Schreiner, F. Neumann, M. Neumann, A. End, S.M. Roedler, S. Aharinejad, The influence of optimization target selection on the structure of arterial tree models generated by constrained constructive optimization, J. Gen. Physiol. 106 (1995) 583–599.
[14] W. Schreiner, F. Neumann, M. Neumann, R. Karch, A. End, S.M. Roedler, Limited bifurcation asymmetry in coronary arterial tree models generated by constrained constructive optimization, J. Gen. Physiol. 109 (1997) 129–140.
[15] W. Schreiner, F. Neumann, M. Neumann, A. End, M.R. Müller, Structural quantification and bifurcation symmetry in arterial tree models generated by constrained constructive optimization, J. Theor. Biol. 180 (1996) 161–174.
[16] F. Neumann, W. Schreiner, M. Neumann, Computer simulation of coronary arterial trees, Adv. Eng. Software 28 (1997) 353–357.
[17] J.B. Bassingthwaighte, R.B. King, S.A. Roger, Fractal nature of regional myocardial blood flow heterogeneity, Circ. Res. 65 (1989) 578–590.
[18] P.O. Iversen, G. Nicolaysen, Fractals describe blood flow heterogeneity within skeletal muscle and within myocardium, Am. J. Physiol. 268 (1995) H112–H116 (Heart Circ. Physiol. 37).
[19] Y. C. Fung, Biomechanics: Circulation, Springer-Verlag, New York, 1984, p. 11.
[20] T.F. Sherman, On connecting large vessels to small: the meaning of Murray's law, J. Gen. Physiol. 78 (1981) 431–453.
[21] G.S. Kassab, Y.C.B. Fung, The pattern of coronary arteriolar bifurcations and the uniform shear hypothesis, Ann. Biomed. Eng. 23 (1995) 13–20.
[22] W. Schreiner, P. Buxbaum, Computer-optimization of vascular trees, IEEE Trans. Biomed. Eng. 40 (1993) 482–491.
[23] M. LaBarbera, Principles of design of fluid transport systems in zoology, Science 249 (1990) 992–999.
[24] C.D. Murray, The physiological principle of minimum work applied to the angle of branching of arteries, J. Gen. Physiol. 9 (1926) 835–841.
[25] D. W. Thompson, On Growth and Form (reprint of the 2nd edition, Cambridge, 1942), Dover, Mineola, NY, 1992, pp. 948–957.
[26] R. Rosen, Optimality Principles in Biology, Butterworth, London, 1967, pp. 40–60.

[27] A. Kamiya, T. Togawa, Optimal branching structure of the vascular tree, Bull. Math. Biophys. 34 (1972) 431–438.
[28] M. Zamir, Optimality principles in arterial branching, J. Theor. Biol. 62 (1976) 227–251.
[29] D.L. Kohn, Optimal systems. I. The vascular system, Bull. Math. Biophys. 16 (1954) 59–74.
[30] A. Kamiya, T. Togawa, A. Yamamoto, Theoretical relationship between the optimal models of the vascular tree, Bull. Math. Biol. 36 (1974) 311–323.
[31] M. Zamir, The role of shear forces in arterial branching, J. Gen. Physiol. 67 (1976) 213–222.
[32] H.B.M. Uylings, Optimization of diameters and bifurcation angles in lung and vascular tree structures, Bull. Math. Biol. 39 (1977) 509–519.
[33] J. Lefèvre, Teleonomical optimization of a fractal model of the pulmonary arterial bed, J. Theor. Biol. 102 (1983) 225–248.
[34] G.B. West, J.H. Brown, B.J. Enquist, A general model for the origin of allometric scaling laws in biology, Science 276 (1997) 122–126.
[35] M. Zamir, H. Chee, Branching characteristics of human coronary arteries, Can. J. Physiol. Pharmacol. 64 (1986) 661–668.
[36] D. Knuth, The Art of Computer Programming, vol. 1, Fundamental Algorithms, 2nd ed., Addison-Wesley, Reading, MA, 1973, pp. 305–332.
[37] The Numerical Algorithms Group, NAG Fortran Library Manual Mark 16, The Numerical Algorithms Group Ltd, Oxford, UK, 1993.
[38] M. Zamir, Distributing and delivering vessels of the human heart, J. Gen. Physiol. 91 (1988) 725–735.
[39] M. Zamir, H. Chee, Segment analysis of human coronary arteries, Blood Vessels 24 (1987) 76–84.
[40] F. Neumann, M. Neumann, R. Karch, W. Schreiner, Visualization of computer-generated arterial model trees, in: M. Cerrolaza, D. Jugo, C.A. Brebbia (Eds.), BIOSIM 96, Proceedings of the 1st Int. Conf. on Simulation Modelling in Bioengineering, Mérida, Venezuela, 1996, Computational Mechanics Publications, Southampton, 1996, pp. 259–268.
[41] A. Kamiya, T. Togawa, Adaptive regulation of wall shear stress to flow change in the canine carotid artery, Am. J. Physiol. 239 (1980) H14–H21.
[42] R.D. Brownlee, B.L. Langille, Arterial adaptations to altered blood flow, Can. J. Physiol. Pharmacol. 69 (1991) 978–983.
[43] Y. Kouchi, Y. Onuki, M.H. Wu, Q. Shi, L.R. Sauvage, Effect of altered blood flow on the caliber and morphology of the internal thoracic artery in the dog, J. Thorac. Cardiovasc. Surg. 113 (1997) 114–120.
[44] X. Girerd, G. London, P. Boutouyrie, J.J. Mourad, M. Safar, S. Laurent, Remodeling of the radial artery in response to a chronic increase in shear stress, Hypertension 27 (1996) 799–803.
[45] O. Hudlicka, A.J. Wright, A.M. Ziada, Angiogenesis in the heart and skeletal muscle, Can. J. Cardiol. 2 (1986) 120–123.
[46] O. Hudlicka, Mechanical factors involved in the growth of the heart and its blood vessels, Cell Mol. Biol. Res. 40 (1994) 143–152.

Rudolf Karch studied Physics and Mathematics and received his PhD in Physics from the University of Vienna, Austria, in 1995. In 1996 he joined the group for Biomedical Computer Simulation at the Department of Medical Computer Sciences, University of Vienna. His main research interests are computer simulations in biomedicine.

Friederike Neumann received her PhD in Psychology and Statistics from the University of Vienna, Austria, in 1975. She was involved in numerous research projects in the social sciences, and later in clinical research with the main interest on signal processing and statistical analysis of physiological data. In 1994 she joined the research group for Biomedical Computer Simulation at the Department of Medical Computer Sciences, with her research activities mostly dedicated to statistical data analysis of simulated vascular structures.

Martin Neumann studied Physics and Mathematics and received his PhD in Physics from the University of Vienna, Austria, in 1979. After a postdoctoral position at the Catholic University of America, Washington DC, 1979–1981, he joined the staff of the Institute of Experimental Physics of the University of Vienna. He has also worked as a research fellow in Parallel Computing at the University of Edinburgh, Scotland, in 1983, and as Visiting Professor at the University of Florence, Italy, in 1990. In 1989, he

was awarded the Ludwig Boltzmann Prize by the Austrian Physical Society. He is currently Associate Professor of Statistical Physics at the Institute of Experimental Physics and co-founder of that Institute's Computational Physics Group.

His main research interests are in the field of Molecular Simulation and Visualization, including systems with long-range interactions, associating liquids, supercritical mixtures, and quantum mechanical simulations. His cooperation with the group for Biomedical Computer Simulation at the Department of Medical Computer Sciences has been established in 1993. Here, his interests are the numerical hemodynamics in vascular systems and the visualization of complex tree structures.

Wolfgang Schreiner studied Physics and Mathematics and received his PhD in Physics from the University of Vienna, Austria, in 1979. He worked on the computer simulation of liquids, first as a research fellow at London University and then as assistant at the Institute of Experimental Physics at Vienna University. He was coauthor on a monography in the field of nuclear medicine. Since 1984 he has been head of the section for computerized analysis of medical data at the Second Department of Surgery, University of Vienna, and in 1991 he was appointed head of a working group for Biomedical Computer Simulation. In 1995 he was appointed full professor of Medical Informatics at the University of Vienna. His main research fields include biomedical computer simulation, modeling, and biomathematics.